Structural Contributions to Second-Order Optical Nonlinearities in Oriented Interfacial Multilayers

W. C. Flory,[†] S. M. Mehrens, and G. J. Blanchard*,[‡]

Contribution from the Department of Chemistry, Michigan State University, East Lansing, Michigan 48824-1322

Received January 21, 2000

Abstract: We report on the synthesis and characterization of Zr-phosphate/phosphonate (ZP) self-assembled multilayer structures using surface second harmonic generation measurements. We use two structurally complementary $\chi^{(2)}$-active chromophores that can be deposited with orientational control relative to the substrate. These chromophores produce multilayer $\chi^{(2)}$ responses identical in magnitude but of opposite sign. We form opposing bilayers with these chromophores to produce two different structural motifs, each with a local center of inversion about the ZP interlayer bonding plane. The $\chi^{(2)}$ responses of these two bilayer systems are different and reveal the extent to which the dipole approximation is valid in these layered assemblies. Our data elucidate the role that quadrupolar terms play in the $\chi^{(2)}$ responses of thin interfacial films. This work illustrates the complex and subtle structural issues associated with the design and construction of layered interfaces and provides a means to evaluate the vacancy and orientational defect density in layered materials.

Introduction

Self-assembled mono- and multilayer structures (SAMs) have received a great deal of attention in the materials community for fundamental as well as more near-term reasons.[1−9] An overarching goal of this effort has been to make the connection between molecular-scale organization, interface chemical identity, and macroscopic materials properties. A tremendous amount has been learned about interfacial monolayers and the associated measurement technology using the alkanethiol/gold system.[10−12] While studies of this archetypal system have led to profound advances in our understanding of organic-modified interfaces, thiol/gold monolayers suffer from long-term chemical stability limitations[13,14] and, until recently, the inability to form chemically bound multilayer assemblies.[15] These limitations have been a driving force for research to identify alternative layer growth strategies, with both silane[2,16−19] and Zr-phosphate/phosphonate (ZP) chemistry[1,19−34] proving successful and versatile. The interest in SAMs based on ZP interlayer linking chemistry arises from their ease of assembly, the mild conditions used in the formation of these layers, and their structural and thermal stability, once formed.

Recent work on ZP-based SAMs has pointed to limitations in their properties (e.g., mesoscopic ordering, optical response)

[†] Present address: Colorado State University, Department of Chemistry, Fort Collins, CO 80523.

[‡] To whom correspondence should be addressed. E-mail address: blanchard@photon.cem.msu.edu.

(1) Katz, H. E.; Scheller, G.; Putvinski, T. M.; Schilling, M. L.; Wilson, W. L.; Chidsey, C. E. D. *Science* **1991**, *254*, 1485.
(2) Li, D.; Ratner, M. A.; Marks, T. J.; Zhang, C. H.; Yang, J.; Wong, G. K. *J. Am. Chem. Soc.* **1990**, *112*, 7389.
(3) Kepley, L. J.; Crooks, R. M.; Ricco, A. *Anal. Chem.* **1992**, *64*, 3191.
(4) Swalen, J. P.; Allara, D. L.; Andrade, J. P.; Chandross, E. A.; Garoff, S.; Israelachvilli, J.; McCarthy, T. J.; Murray, R.; Pease, R. F.; Rabolt, J. F.; Wynne, K. J.; Tu, H. *Langmuir* **1987**, *3*, 932.
(5) Calvert, J. M.; Georger, J. H., Jr.; Peckerer, M. C.; Perhsson, P. E.; Schnur, J. M.; Scheon, P. E. *Thin Films* **1992**, *114*, 9188.
(6) Dulcey, C. S.; Georger, J. H.; Krauthamer, V.; Stenger, D. A.; Fare, T. L.; Calvert, J. M. *Science* **1991**, *252*, 551.
(7) Kumar, A.; Biebuyck, H. A.; Abbott, N. L.; Whitesides, G. M. *J. Am. Chem. Soc.* **1992**, *114*, 9188.
(8) Vrancken, K. C.; Van Der Voort, P.; Gillis-D'Hammers, I.; Vansant, E. F.; Grobet, P. *J. Chem. Soc., Faraday Trans.* **1992**, *88*, 3197.
(9) Pfleiderer, B.; Albert, K.; Bayer, E. *J. Chromatogr.* **1990**, *506*, 343.
(10) Ulman, A. *Chem. Rev.* **1996**, *96*, 1533.
(11) Dubois, L. H.; Nuzzo, R. G. *Annu. Rev. Phys. Chem.* **1992**, *43*, 437.
(12) Xia, Y.; Whitesides, G. M. *Angew. Chem., Int. Ed.* **1998**, *37*, 551.
(13) Karpovich, D. S.; Blanchard, G. J. *Langmuir* **1994**, *10*, 3315.
(14) Schessler, H. M.; Karpovich, D. S.; Blanchard, G. J. *J. Am. Chem. Soc.* **1996**, *118*, 9645.
(15) Kohli, P.; Taylor, K. K.; Harris, J. J.; Blanchard, G. J. *J. Am. Chem. Soc.* **1998**, *120*, 11962.
(16) Gun, J.; Iscovici, R.; Sagiv, J. *J. Colloid Interface Sci* **1984**, *101*, 201.
(17) Maoz, R.; Sagiv, J. *Thin Solid Films* **1985**, *132*, 135.
(18) Maoz, R.; Sagiv, J. *Thin Solid Films* **1985**, *132*, 135.
(19) Hong, H.-G.; Sackett, D. D.; Mallouk, T. E. *Chem. Mater.* **1991**, *3*, 521.
(20) Thompson, M. E. *Chem. Mater.* **1994**, *6*, 1168.
(21) Katz, H. E.; Wilson, W. L.; Scheller, G. *J. Am. Chem. Soc.* **1994**, *116*, 6636.
(22) Yonemoto, E. H.; Saupe, G. B.; Schmehl, R. H.; Hubig, S. M.; Riley, R. L.; Iverson, B. L.; Mallouk, T. E. *J. Am. Chem. Soc.* **1994**, *116*, 4786.
(23) Katz, H. E.; Bent, S. F.; Wilson, W. L.; Schilling, M. L.; Ungashe, S. B. *J. Am. Chem. Soc.* **1994**, *116*, 6631.
(24) Frey, B. L.; Hanken, D. G.; Corn, R. M. *Langmuir* **1993**, *9*, 1815.
(25) Yang, H. C.; Aoki, K.; Hong, H.-G.; Sackett, D. D.; Arendt, M. F.; Yau, S.-L.; Bell, C. M.; Mallouk, T. E. *J. Am. Chem. Soc.* **1993**, *115*, 11855.
(26) Vermeulen, L.; Thompson, M. E. *Nature* **1992**, *358*, 656.
(27) Ungashe, S. B.; Wilson, W. L.; Katz, H. E.; Scheller, G. R.; Putvinski, T. M. *J. Am. Chem. Soc.* **1992**, *114*, 8717.
(28) Cao, G.; Rabenberg, L. K.; Nunn, C. M.; Mallouk, T. M. *Chem. Mater.* **1991**, *3*, 149.
(29) Katz, H. E.; Schilling, M. L.; Chidsey, C. E. D.; Putvinski, T. M.; Hutton, R. S. *Chem. Mater.* **1991**, *3*, 699.
(30) Putvinski, T. M.; Schilling, M. L.; Katz, H. E.; Chidsey, C. E. D.; Mujsce, A. M.; Emerson, A. B. *Langmuir* **1990**, *6*, 1567.
(31) Rong, D.; Hong, H.-G.; Kim, Y.-I.; Krueger, J. S.; Mayer, J. E.; Mallouk, T. E. *Coord. Chem. Rev.* **1990**, *97*, 237.
(32) Lee, H.; Kepley, L. J.; Hong, H.-G.; Akhter, S.; Mallouk, T. E. *J. Phys. Chem.* **1988**, *92*, 2597.
(33) Lee, H.; Kepley, L. J.; Hong, H.-G.; Mallouk, T. E. *J. Am. Chem. Soc.* **1988**, *110*, 618.
(34) Katz, H. E. *Chem. Mater.* **1994**, *6*, 2227.

10.1021/ja000232y CCC: $19.00
Published on Web 07/28/2000

that are mediated by structural defects.[35,36] The characterization of defects in mono- and multilayer interfaces is central to understanding SAM properties and is an area of interface and materials science that remains to be explored more fully. For alkanethiol/gold monolayers, cyclic voltammetry and impedance measurements have proven to be valuable tools in detecting the presence of vacancy defects.[37−42] For multilayers, electrochemical methods are not generally as useful owing to the short-range nature of the electron tunneling process responsible for the experimental signal. We are investigating a means to study defects in multilayer assemblies using nonlinear spectroscopic methods. For many optical methods, the characteristic response of surface defects is small compared to the bulk material contribution, limiting the utility of spectroscopy for such investigations. We are interested in measuring vacancy and substitution defects in layered interfaces by utilizing the functional chemistry of selected second-order nonlinear chromophores to control their orientation during layer growth. We have chosen $\chi^{(2)}$ measurements because of their intrinsic surface-selectivity.[43] By constructing interfaces with specific, predetermined orientation of the chromophore nonlinear transition moment within each layer, multilayer films can be assembled to produce either centrosymmetric or noncentrosymmetric bulk ordering, to first approximation. The $\chi^{(2)}$ nonlinear response of a centrosymmetric bilayer structure will be null to within the validity of the electric dipole approximation. This dipolar cancellation allows examination of the residual $\chi^{(2)}$ response in the context of vacancy and substitution defects and higher order multipole contributions to the experimental signal against a nominally dark background. The resolution of the contributions of opposing bilayers to the $\chi^{(2)}$ response is an important first step in establishing this means of defect characterization in layered materials.

We use two compounds to explore the utility and practical limitations of chemically based cancellation of the second-order nonlinear response. The first is the $\chi^{(2)}$-chromophore (4-(4-(4-(4-((2-hydroxyethyl)sulfonyl)phenyl)azo)phenyl)piperazinyl)-phenyl)phosphonic acid **(1)**, reported by Katz and co-workers and designed for its combined rigid structure and large first hyperpolarizability, β.[21] The second compound, (2-(4-(4-(4-(4-hydroxyphenyl)piperazinyl)-phenyl)azophenyl)sulfonyl)-ethylphosphonic acid **(2)**, is the structural complement of **1**, where the functional groups at the termini have been exchanged. The synthetic route to **2** is reported here and the structures of both molecules are shown in Figure 1. We report on the surface second harmonic generation (SSHG) response of multilayer assemblies of these chromophores for several different bilayer structural arrangements. Following a discussion of the experimental details, we consider the results of our experiments on these complementary chromophores in the context of the physical and chemical origins of the nonlinear response. We discuss the form of the SSHG signal and how that signal is related to the several contributions to the second-order nonlinear susceptibility, $\chi^{(2)}$. We find direct evidence for the role of electric quadrupolar contributions to our data, with the magnitude of the quadrupole contribution depending sensitively on the chemical functionality in the vicinity of the ZP linking moieties.

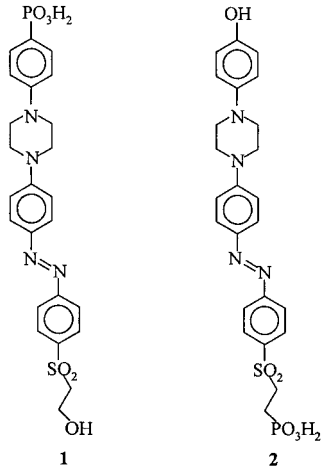

Figure 1. Structures of chromophores **1** and **2**.

Experimental Section

Chemicals. All chemicals used were obtained in the highest purity grade available. (4-Acetylaminobenzene)sulfonyl chloride, 2-chloroethanol, 2,3,4-collidine, $POCl_3$, $ZrOCl_2 \cdot 8H_2O$, triisopropyl phosphite, *p*-anisidine, bromotrimethylsilane, and $CDCl_3$ were obtained from Aldrich Chemical Co. *p*-Toluenesulfonyl chloride, sodium sulfite, and sodium bisulfite were obtained from Spectrum Chemicals. *N*,*N*-Bis-2-chloroethanol was obtained from Pfaltz & Bauer, d_6-DMSO was purchased from Isotec Inc., and 3-aminopropyltrimethoxysilane was purchased from United Chemical Technologies, Inc. All water used was distilled in-house. All chemicals were used as received except for triisopropyl phosphite, which was purified by drying over sodium under an inert atmosphere followed by vacuum distillation.[44]

Synthesis. The synthesis of chromophore **1** has been reported previously.[21] The details of the synthetic route for chromophore **2** are provided as Supporting Information to this paper.

Surface Preparation. Si(100) wafers (Multi Crystal Optics, Inc.) and silica substrates were used. Si substrates were cleaned in a piranha solution (3:1 H_2SO_4:H_2O_2. *Caution—strong oxidizer!*) for 10 min, rinsed with distilled water, placed in 2 M HCl for 10 min, and rinsed with water. The substrates were dried in a dry N_2 stream. Under an Ar atmosphere, 20 mL of anhydrous octane was added to a vessel containing the substrate. The octane was heated to reflux, and 3-aminopropyltrimethoxysilane was added to make a 1% v/v solution. After 10 min of reaction the substrate was removed and rinsed with warm hexane and then water. A N_2 stream was used to dry the surface. Silica surfaces were cleaned in piranha solution and dried, but they were not primed. Both surfaces were then phosphorylated. This was done under Ar, using a solution of 20 mM 2,3,4-collidine and 20 mM $POCl_3$ in anhydrous acetonitrile at ambient temperature. After 10 min, the substrates were removed, rinsed with acetonitrile and water, and dried with N_2. The surfaces were then zirconated by being immersed in an aqueous 5 mM $ZrOCl_2$ solution for 10 min. The surfaces were rinsed with water and dried.

Chromophore Deposition. Chromophores **1** and **2** were deposited on zirconated substrates from a saturated solution ($\sim$ 0.2 mM) of the appropriate chromophore dissolved in 1:4 DMF:EtOH. Deposition of each layer was from a solution containing either **1** or **2**, but not both. The temperature of each deposition solution was maintained slightly below boiling while the zirconated substrates were immersed for 10 min, followed by rinsing with warm ethanol and drying with N_2. Subsequent phosphorylation and zirconation of the chromophore-containing surfaces was performed as described above. Before measure-

(35) Horne, J. C.; Huang, Y.; Liu, G.-Y.; Blanchard, G. J. *J. Am. Chem. Soc.* **1999**, *121*, 4419.
(36) Horne, J. C.; Blanchard, G. J. *J. Am. Chem. Soc.* **1999**, *121*, 4427.
(37) Sabatini, E.; Rubinstein, I. *J. Phys. Chem.* **1987**, *91*, 6663.
(38) Sabatini, E.; Rubinstein, I.; Moaz, R.; Sagiv, J. *J. Electroanal. Chem.* **1987**, *219*, 365.
(39) Finklea, H. O.; Snider, D. A.; Fedyk, J.; Sabatini, E.; Gafni, Y.; Rubinstein, I. *Langmuir* **1993**, *9*, 3660.
(40) Finklea, H. O.; Snider, D. A.; Fedyk, J. *Langmuir* **1990**, *6*, 371.
(41) Sabatini, E.; Cohen-Boulakia, J.; Bruening, M. L.; Rubinstein, I. *Langmuir* **1993**, *9*, 2974.
(42) Janek, R. P.; Fawcett, W. R.; Ulman, A. *Langmuir* **1998**, *14*, 3011.
(43) Shen, Y. R. *The Principles of Nonlinear Optics*; John Wiley and Sons: New York, 1984.
(44) Perrin, D. D.; Armarego, W. L. F.; Perrin, B. R. *Purification of Individual Organic Chemicals*; Pergmon Press: Oxford, 1980; p 449.

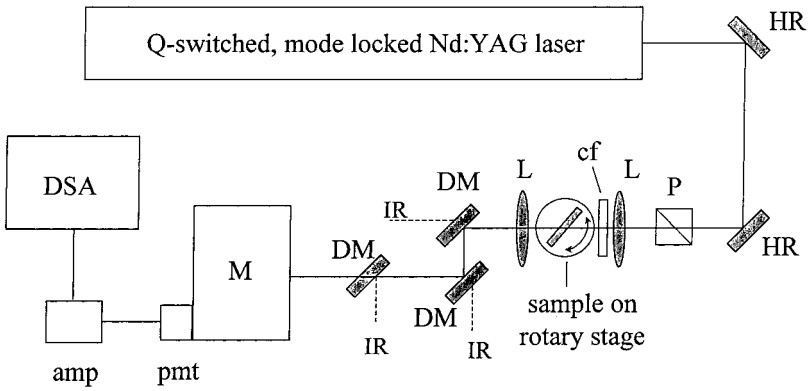

Figure 2. Surface SHG laser system based on a mode-locked, Q-switched Nd:YAG laser. Abbreviations: HR = high reflector, P = polarization rotator, L = lens, cf = color filter, DM = dichroic mirror, M = monochromator, pmt = photomultiplier detector, amp = amplifier, DSA = digital signal analyzer.

ment of adlayers for $\chi^{(2)}$ activity, terminal OH groups were phosphorylated. To monitor layer adsorption, the UV−visible absorbance spectrum of the sample was measured after each deposition cycle, and in all cases linear growth was observed.

Measurements. ^{1}H NMR spectra of all compounds were taken with a Varian Gemini-300 MHz NMR spectrometer. Optical absorption measurements were made using a Hitachi U-4001 UV−visible absorption spectrometer. The thickness of chromophore layers bound to Si substrates was measured using an optical null ellipsometer (Rudolph AutoEL-II) operating at $\lambda = 632.8$ nm. The software used to calculate layer thickness was supplied by Rudolph. The complex refractive index of the individual layers was taken to be $n = 1.61 + 0i$.[45]

Calculations. Semiempirical and molecular mechanics calculations were performed on chromophores **1** and **2** using Hyperchem v. 4.5 on a PC. Energy level calculations were performed on ground-state-optimized structures using the PM3 parametrization.

Surface Second Harmonic Generation Laser System. A schematic of the surface SHG system is shown in Figure 2. A Q-switched, mode-locked Nd:YAG laser (Quantronix model 416) produces ~1.4 W average power at 1064 nm with a 2 μs envelope at 500 Hz. The mode-locked pulses (80 MHz repetition rate) within the 2 μs envelope are characterized by a 100 ps pulse width. The 1064 nm pulse train is directed through a 2 mm spatial filter and a polarization rotator and then through a focusing lens and a color filter (RG 610) to remove any 532 nm light generated by the optics. The 1064 nm beam is focused onto the sample (~100 μm diameter spot size) and is then recollimated. After the recollimating lens, three dichroic mirrors are used to separate the fundamental from the second harmonic light. The second harmonic light is directed into a 0.25 m monochromator (Fisher) and is detected with a PMT (Hamamatsu 466). The resulting transient is amplified (Ortec model 451) and then stored using a digital signal analyzer (Textronix DSA 602A). The sample is located at the focal point of the fundamental laser beam and is rotated manually about its vertical (y) axis from 0° to 70° relative to the incident beam using a precision rotation stage (Newport 481 A). Each experimental datum point is the result of three individual readings, with each reading being an average of 532 scans of the amplified transient recorded by the digital signal analyzer. The complete scan is normalized by referencing it to a scan of a reference bare fused silica substrate.

Results and Discussion

The purpose of this paper is to evaluate the use of structural cancellation at interfaces as a means of creating a nominally null $\chi^{(2)}$ background, making possible the characterization of interface vacancy and orientational defect density. We first report on the characterization of these layers by UV−visible absorbance and optical ellipsometry. We then provide an overview of the relevant theory and discuss our experimental findings in the context of the contributions to the angle-dependent surface SHG data. We consider the nonlinear response of the bare fused silica substrate first and then the same surface with layers of each chromophore adsorbed. With that information in hand, we present our data on two opposing bilayer structures: [SiO_x-**1**-**2**] and [SiO_x-**2**-**1**]. Their SSHG responses are not identical, pointing to the role and chemical identity of an adlayer quadrupole contribution to the experimental signal.

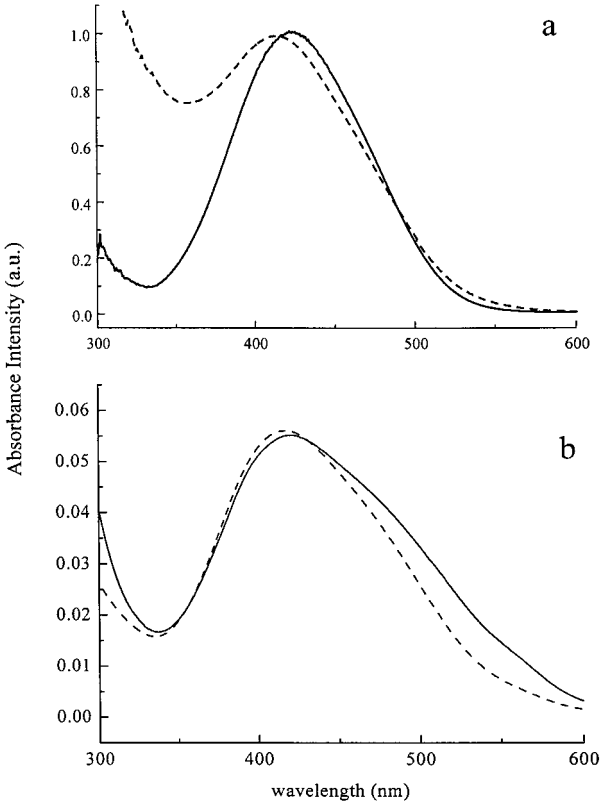

Figure 3. The UV−visible absorption spectra of (a) solution phase of **1** (solid line) and **2** (dashed line) and (b) the assemblies of five bilayers of **1** and **2** on fused silica.

The linear optical responses of chromophores **1** and **2** in ethanol are shown in Figure 3a. The absorption maxima for **1** and **2** in solution are 429 and 415 nm, respectively. The slight difference between the two chromophores is due to the position of the terminal functional groups and the influence each has on the π system of the chromophores. We have assembled layers of **1** and **2** separately on SiO_x substrates. We show the absorption spectra of layers of chromophores **1** and **2** in Figure 3b,

(45) Hanken, Dennis G.; Corn, Robert M. *Anal. Chem.* **1995**, *67*, 3767.

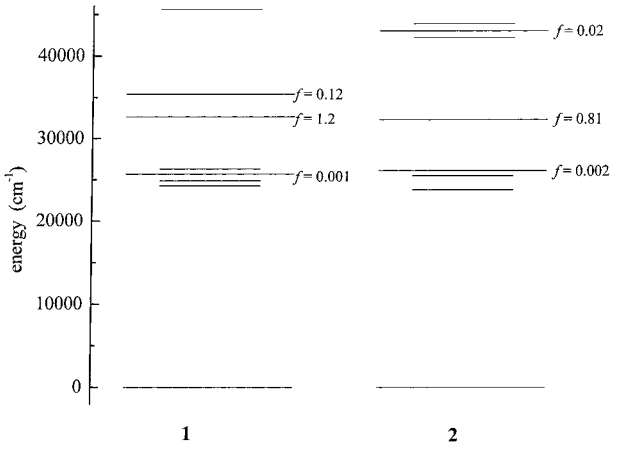

Figure 4. Semiempirical calculations of the linear response for chromophores **1** (left) and **2** (right). Wide lines are singlet states, and calculated oscillator strengths for $S_i \leftarrow S_0$ transitions are indicated next to the upper state. Narrower lines indicate triplet states.

revealing very similar electronic structures. Both chromophores are dominated by a broad absorption band centered at 417 nm, with only very slight differences in the red edge of the spectra. The higher energy bands appear to be somewhat different for the two chromophores, and the reason for this effect is not obvious by inspection. Semiempirical calculations of the linear response for these two chromophores show the ordering and energies of the first three excited singlet states to be slightly different, especially in the region of the most prominent band-(s) (Figure 4). These calculations provide some justification for the differences in the absorption data, but given the spectral widths of the absorption bands, making the comparison between experiment and calculation at any meaningful level is not feasible. By plotting the absorbance of each chromophore at 417 nm against the number of deposited layers, we recover slopes of 0.0567 ± 0.001 and 0.0546 ± 0.0007 for **1** and **2**, respectively, as shown in Figure 5a. These data demonstrate that the same density of chromophores is deposited in each layer, an important result for future uses of these chromophores in nonlinear applications (vide infra). Because linear growth is seen for each layer, we also conclude that priming the surface prior to chromophore deposition does not yield a more uniform surface coverage. From the solution phase spectra, we extract $\epsilon_{max} = 207\,600$ L/mol-cm for **1**, and given the same linear dependence of absorbance on layer growth for **2**, we infer the same value of ϵ. Using the experimental data shown in Figure 5a, we estimate the surface loading density to be 1.6×10^{14} cm^{-2}-layer^{-1}.

From optical null ellipsometry, we recover a best fit slope of 26.3 ± 0.5 Å/layer for chromophore **1** and 25.5 ± 0.4 Å/layer for chromophore **2** (Figure 5b). These values are the same to within the experimental uncertainty. Our results are in good agreement with Katz data on the layered growth of **1**.[1] The length of each molecule in its most stable conformation is calculated by molecular mechanics to be 27 Å. It has been reported previously that the thickness of a Zr−PO_3^- linkage is 3.75 Å.[29] An average layer thickness of 25.6 Å indicates that the chromophores are tilted at an angle of ∼20° from the surface normal, presuming full surface coverage. Katz also reported this result for **1**.[1] Because both chromophores tilt at similar angles when incorporated into a layer, it can be assumed that assemblies of alternating layers of **1** and **2** will result in a linear increase in the layer thickness.

These chromophores are characterized by the same layer density, electronic structure, and tilt angle on the basis of the linear response and ellipsometry data. We conclude that multilayers of **1** and **2** are structurally similar, making them a good choice for investigations of the chemical structural contributions to the $\chi^{(2)}$ response of oriented ZP systems. With this information in hand, we consider the surface SHG experiments next.

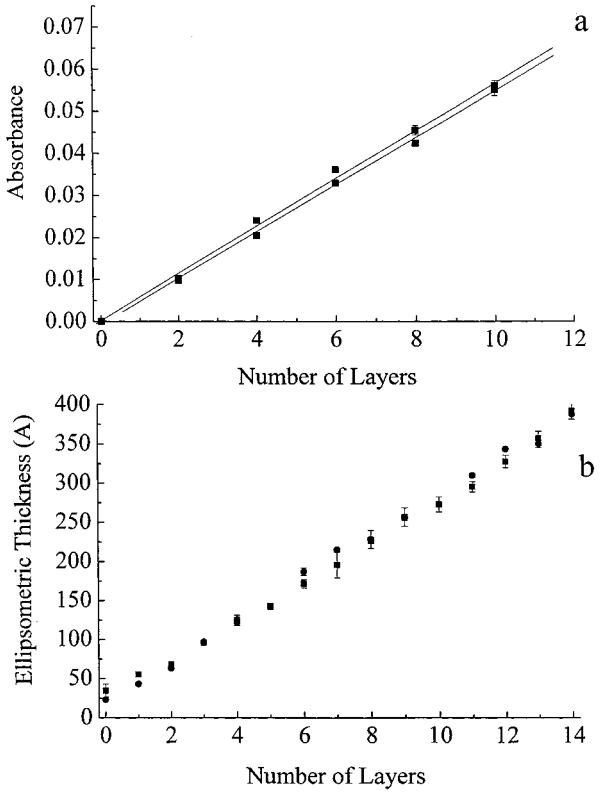

Figure 5. (a) Dependence of absorption on number of layers for both chromophores. See text for a discussion of these data. (b) Ellipsometric thicknesses of each layer for 15 layer assemblies of chromophores **1** (●) and **2** (■). The slopes of the best-fit line through these data are 26.3 ± 0.5 Å/layer for **1** and 25.5 ± 0.4 Å/layer for **2**. The *y*-intercept is a result of the primer layer.

Many surface SHG experiments are performed in the reflection mode,[46−49] with the angle of incidence of the fundamental electric field being the independent experimental variable. The form of the signal in these experiments is an incidence-angle dependent intensity of the reflected second harmonic light. The specific form of the data can, under favorable circumstances, be used to estimate the average tilt angle of the nonlinear chromophore relative to the surface normal and the magnitude of the experimental signal can be used to determine the value(s) of selected $\chi^{(2)}$ tensor elements. For SSHG transmission measurements on transparent substrates,[50−54] such as those we

(46) Heinz, T. F.; Tom, H. W. K.; Shen, Y. R. *Phys. Rev. A.* **1983**, *28*, 1883.
(47) Bloembergen, N.; Chang, R. K.; Jha, S. S.; Lee, C. H. *Phys. Rev.* **1968**, *174*, 813.
(48) Naujok, R. R.; Higgins, D. A.; Hanken, D. G.; Corn, R. M. *J. Chem. Soc., Faraday Trans.* **1995**, *91*, 1411.
(49) Daschbach, J. L.; Fischer, P. R.; Gragson, D. E.; Demarest, D.; Richmond, G. L. *J. Phys. Chem.* **1995**, *99*, 10690.
(50) Lupo, D.; Prass, W.; Scheunemann, U.; Laschewsky, A.; Ringsdorf, H.; Ledoux, I. *J. Opt. Soc. Am. B* **1988**, *5*, 300.
(51) Berkovic, G.; Shen, Y. R.; Marowsky, G.; Steinhoff, R. *J. Opt. Soc. Am. B* **1989**, *6*, 205.
(52) Sato, O.; Baba, R.; Hashimoto, K.; Fujishima, A. *J. Electroanal. Chem.* **1991**, *306*, 291.
(53) Kajikawa, K.; Takezoe, H.; Fukuda, A. *Chem. Phys. Lett.* **1993**, *205*, 225.
(54) Herman, W.; Hayden, L. M. *J. Opt. Soc. Am. B* **1995**, *12*, 416.

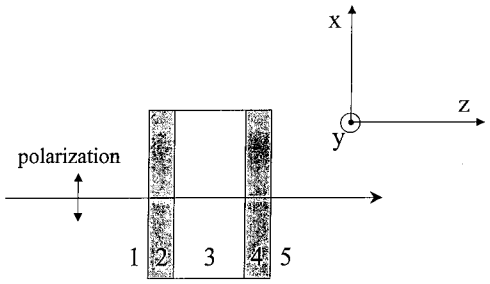

Figure 6. Model system of thin films on both sides of a substrate: 1 and 5 are air; 2 and 4 are interfacial thin films; 3 is the substrate.

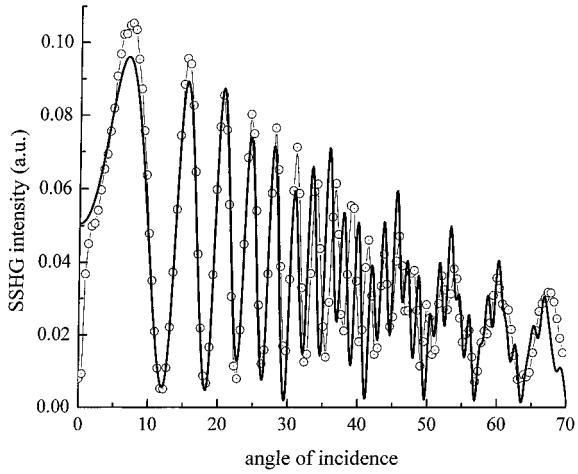

Figure 7. Surface SHG for a clean fused-silica substrate vs angle of sample rotation (0° is the condition where the incident electric field is propagates along the surface normal axis) plotted with the model for three components of the etalon effect.

report here, the form of the experimental signal is somewhat more complicated and optical interference and transmission/reflection effects must be accounted for. We detail these effects below and discuss how information on interface properties can be obtained from our data.

We consider the system shown in Figure 6, where the incident electric field at frequency ω and polarized along the *x*-axis (p-polarized) and propagates along the *z*-axis. For this experiment, we collect the second harmonic signal over both s- and p-polarizations. The sample, composed of a transparent substrate, has interfacial layers present on both the front and back surfaces. The sample is rotated about the *y*-axis, and the resultant second harmonic signal intensity is recorded as a function of rotation angle. Four effects contribute to the data. The first is the angle dependence of the reflection and transmission properties of the sample at both the fundamental and second harmonic frequencies. The second effect is optical interference between second harmonic light generated at the front and back faces of the sample. Both the first and second effects are understood in the context of simple optical phenomena. The third and fourth features are the magnitude and shape of the envelope function of the SHG data. These quantities are related to the second-order nonlinear susceptibility, $\chi^{(2)}$, and the orientation and angular distribution of the dominant $\chi^{(2)}$ tensor element(s) for the sample under consideration.

Optical Effects. The angular dependence of the SHG signal we recover is oscillatory with respect to the angle of incidence of the fundamental electric field (Figure 7). This pattern appears to be outwardly similar to that produced by Maker fringes,[54−56] but it cannot be accounted for using Maker's treatment because the coherence length of the light source we use is long relative to the thickness of the portion of the sample that generates the second harmonic signal. The origin of the oscillatory signal shown in Figure 7 is interference between the second harmonic light generated at the front and back interfaces of the transparent substrate.[50,52,53]

For the model system shown in Figure 6, we can decompose the induced polarization at 2ω into the components that arise from nonlinear interactions at each interface (layers 2 and 4 in Figure 6),[57,58]

$$E^{2\omega} = E_2^{2\omega} + E_4^{2\omega} \tag{1}$$

For $E^{2\omega}$ generated at each interface, we must account for the angular dependence of reflection and transmission, dispersion in each of the media, and the thickness of the interface layer.

$$E_2^{2\omega} = (E^{\omega})^2 (T_{12}^{\omega} R_2^{\omega})^2 T_{23}^{2\omega} R_2^{2\omega} T_{34}^{2\omega} T_{45}^{2\omega} \left(\frac{4\pi\chi^{(2)}}{(\eta_{f_2}^{\omega})^2 - (\eta_{f_2}^{2\omega})^2}\right) \times \exp(i\phi_{f_2}) \exp\left(il_f \frac{2\omega}{c}\right)(\eta_{f_2}^{\omega} \cos\theta_{f_2}^{\omega} - \eta_{f_2}^{2\omega} \cos\theta_{f_2}^{2\omega}) - 1 \tag{2}$$

$$E_4^{2\omega} = (E^{\omega})^2 (T_{12}^{\omega} R_2^{\omega} T_{23}^{\omega} T_{34}^{\omega} R_4^{\omega})^2 T_{45}^{2\omega} R_4^{2\omega} \left(\frac{4\pi\chi^{(2)}}{(\eta_{f_4}^{\omega})^2 - (\eta_{f_4}^{2\omega})^2}\right) \times \exp(i\phi_{f_4}) \exp\left(il_f \frac{2\omega}{c}\right)(\eta_{f_4}^{\omega} \cos\theta_{f_4}^{\omega} - \eta_{f_4}^{2\omega} \cos\theta_{f_4}^{2\omega}) - 1 \tag{3}$$

where l_f is the film thickness, the terms η are the refractive indices of the films 2 and 4 at the frequencies indicated in the superscripts, the angles θ are the angles of refraction for the layer at the frequencies indicated, and the terms ϕ are the phase angles of the light at 2ω relative to the fundamental at each interface. The *T* and *R* terms are the Fresnel transmittance and reflectance coefficients for a TM-polarized electric field at the interfaces indicated.[59]

$$t_{mn}^{TM} = \frac{2\eta_m \cos\theta_m}{\eta_n \cos\theta_m + \eta_m \cos\theta_n}, \quad T_{mn}^{TM} = \left(\frac{\eta_n \cos\theta_n}{\eta_m \cos\theta_m}\right)(t_{mn}^{TM})^2$$
$$r_{mn}^{TM} = \frac{\eta_n \cos\theta_m - \eta_m \cos\theta_n}{\eta_n \cos\theta_m + \eta_m \cos\theta_n}, \quad R_{mn}^{TM} = (r_{mn}^{TM})^2 \tag{4}$$

The second harmonic light generated at interfaces 2 and 4 is initially in phase with the fundamental electric field at the same interfaces. The term that dominates the observed angular dependence of the signal is the phase mismatch between the second harmonic light generated at interfaces 2 and 4 resulting from dispersion in the substrate. This phase relationship is given by[52]

$$\Delta\phi = (\phi_{f_2} - \phi_{f_4}) = \frac{2\omega}{c} d(\eta_s^{2\omega} \cos\theta_s^{2\omega} - \eta_s^{\omega} \cos\theta_s^{\omega}) \tag{5}$$

where *d* is the substrate thickness. The oscillatory nature of the

(55) Maker, P. D.; Terhune, R. W.; Nisenhoff, M.; Savage, C. M. *Phys. Rev. Lett.* **1962**, *8*, 21.
(56) Jerphagnon, J.; Kurtz, S. K. *J. Appl. Phys.* **1970**, *41*, 1667.
(57) Bloembergen, N.; Pershan, P. S. *Phys. Rev.* **1962**, *128*, 606.
(58) Kajzar, F.; Messier, J.; Zyss, J.; Ledoux, I. *Opt. Commun.* **1983**, *45*, 133.
(59) Pedrotti, F. L.; Pedrotti, L. S. *Introduction to Optics*; Prentice-Hall: 1987; pp 472−487.

signal can be accounted for quantitatively using eq 5. With this information, $I^{2\omega} = (E^{2\omega})^2$ can be calculated as a function of the incidence angle of the fundamental electric field. We show the experimental second-order response of a bare fused silica substrate in Figure 7 along with the calculated signal based on eqs 1−5. We note the presence of several different oscillating components and account for their presence by considering that the substrate will act as an etalon. This is an expected phenomenon. The incident electric field makes multiple passes in the substrate, with the relative contribution from each odd-numbered pass (for a transmission measurement) depending on the angle of incidence in a manner dependent on the flatness of the SiO_x substrate and the Fresnel factors. The data shown in Figure 7 provide important insight into the dominant contributions to the $\chi^{(2)}$ response for this system.

In the interpretation of many second harmonic generation measurements, it is common practice to assume that the electric dipole term in $\chi^{(2)}$ is much larger than the electric quadrupole and higher order terms. While this approximation holds for many experimental conditions, it is not universally the case. For the data we report here, the electric quadrupole term plays a significant role in determining the form of the experimental signal. Guyot-Sionnest and Shen have investigated the contributions of dipolar and quadrupolar terms to the second-order nonlinear susceptibility of surfaces and interfaces.[60] Their work focused on the distinct contributions from the structural and electric field discontinuities that exist where the incident electric field propagates across the interface. In their model, the electric dipole contribution to the $\chi^{(2)}$ response is determined by the structural properties of the interface and they term it a local, intrinsic response. The electric quadrupole term results from the discontinuity experienced by the electric field as it propagates through the interface, and it is termed a nonlocal response because it depends explicitly on the bulk properties of the two phases of matter comprising the interface. Using Guyot-Sionnest and Shen's terminology, the second-order nonlinear susceptibility for an interface is given by[60]

$$\chi^{(2)}_{s\,yzy} = \int_I \left(\chi^{D}_{yzy}(z)s(z) - \frac{\partial}{\partial z}[\chi^{Q}_{zyzy}(z)s(z)] + \chi^{D}_{A,yzzy}(z)\frac{\partial}{\partial z}s(z)\right) dz \quad (6)$$

where $s(z) = 1/\epsilon_i$ ($i = 1,2$, $\epsilon =$ the optical frequency dielectric constant). Before the electric field is incident upon the interface ($z < 0$), $s(z) = 1/\epsilon_1$, and after the interface ($z > 0$), $s(z) = 1/\epsilon_2$. Between these two limits, $s(z)$ varies continuously from $1/\epsilon_1 \rightarrow 1/\epsilon_2$ through the interface. $\chi^{(2)}{}_s$ is the total second-order susceptibility and the integration is over the thickness on the interfacial region. The first term in eq 6 is the electric dipole term associated with the structural properties of the interface, the second is the nonlocal term associated with the induced electric quadrupole moment as the electric field propagates through the interfacial dielectric gradient, and the third term arises from the magnetic dipole moment. The theory is based on the simplest case; an interface between two transparent, nonmagnetic, isotropic media, 1 and 2. For these conditions, the first two terms in eq 6 will contribute most significantly to the observed $\chi^{(2)}{}_s$.

Because the interface electric dipole contribution to the nonlinear susceptibility is an intrinsic property of the material, it can be assumed to be constant over a range of experimental conditions. The discontinuity in the electric field as it propagates through the interface will depend on the difference in ϵ between the two bulk media and this quantity can be varied systematically. Guyot-Sionnest and Shen performed a series of surface SHG measurements using a fused silica substrate immersed in bulk liquids with varying dielectric constants.[60] In this way, the term $\partial/\partial z(s(z))$ could be made small, revealing the role of the electric dipole term, χ^D, for this substrate. They determined from those experiments that the susceptibility of the air-fused silica interface is $\chi^{(2)}{}_s \sim 2.7 \times 10^{-17}$ esu/cm^2, with $\chi^D \sim 5.7 \times 10^{-18}$ esu/cm^2.[60] Although they did not explicitly perform the subtraction owing to the presence of the magnetic dipole term in eq 6, we estimate from their findings that $\chi^Q \sim 2.1 \times 10^{-17}$ esu/cm^2.

With the theoretical framework established by Guyot-Sionnest and Shen in place, we can see from the data in Figure 7 that the envelope function, taken with p-polarized fundamental and collection at 2ω over both p- and s-polarizations, exhibits a signal maximum near normal incidence. For the fused silica substrate, the electric quadrupole term is dominant and the envelope function maximum near normal incidence suggests that the quadrupolar component lies in the plane of the substrate and not perpendicular to it. We expect the detectable portion of the electric dipole contribution to $\chi^{(2)}$ to be aligned with the surface normal (vide infra). We can estimate the resulting "tilt" angle for the bare substrate if we assume that 20% of the total $\chi^{(2)}$ response is from the electric dipole term normal to the surface and 80% of the response is from the electric quadrupole term in the surface plane. The weighted-average would produce an apparent "tilt" angle of 72° with respect to the surface normal for fused silica, and we extract a best fit tilt angle of 63° from our experimental data. The extraction of tilt angle and orientational distribution information from our data is S/N limited, so we view the agreement as good to within the accuracy of these determinations.

Chemical Effects. The chemical properties of the system we sense with surface SHG measurements are the relative magnitudes of the several contributions to the second-order hyperpolarizability of the system and the distribution of orientations of the $\chi^{(2)}$-active species. Recent work by Simpson and Rowlen has treated the issue of $\chi^{(2)}$-chromophore orientation in surface second harmonic generation experiments.[61−63] Among the important findings of their work is that the chromophore tilt angle recovered experimentally converges to an observed "magic angle" of 39.2° with respect to the surface normal as the orientational distribution broadens. The actual treatment of the distribution can be complex, depending on its functional form, and it is typically assumed that the distribution is relatively narrow. In this limit, the dependence of the SHG response on chromophore tilt angle will scale with $\cos^2\langle\theta\rangle$, where $\langle\theta\rangle$ is the average angle between the incident electric field polarization vector and the chromophore nonlinear transition moment. This treatment also assumes that the $\chi^{(2)}$ response is dominated by electric dipole contributions and that the quadrupolar contributions to the experimental signal are negligible. While this is a correct and useful treatment for many systems, we have demonstrated above that we need to also consider quadrupolar terms.

We must consider the orientation and orientational distribution width dependence of the experimental signal for both quadrupolar and dipolar $\chi^{(2)}$ tensors. For this discussion, we assume that the $\chi^{(2)}$ tensors are each dominated by a single element. The only difference between the form of the quadrupolar and dipolar terms lies in the fact that, for interfaces with domain

(60) Guyot-Sionnest, P.; Shen, Y. R. *Phys. Rev. B.* **1987**, *35*, 4420.
(61) Simpson, G. J.; Rowlen, K. L. *J. Am. Chem. Soc.* **1999**, *121*, 2635.
(62) Simpson, G. J.; Rowlen, K. L. *J. Phys. Chem. B* **1999**, *103*, 1525.
(63) Simpson, G. J.; Rowlen, K. L. *J. Phys. Chem. B* **1999**, *103*, 3811.

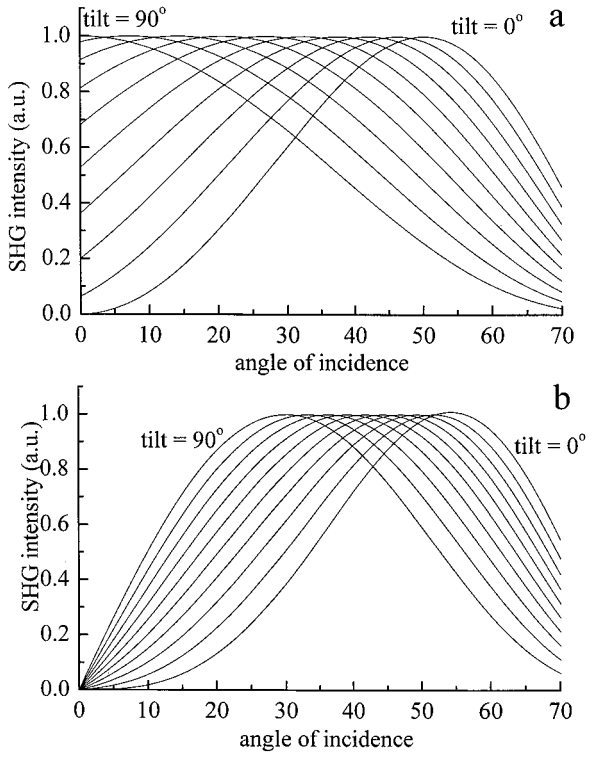

Figure 8. (a) Calculated quadrupolar SSHG envelope function for a series of chromophore tilt angles, as indicated in the plot. (b) Calculated dipolar SSHG envelope function for a series of chromophore tilt angles, as indicated in the plot.

sizes smaller than the diameter of the incident laser beam, there will be dipolar cancellation in the interface plane due to random domain orientation. Thus, only the portion of the dipolar $\chi^{(2)}$ term that projects onto the surface normal vector does not cancel. The situation is fundamentally different for the quadrupolar term because the portions of this term in the interface plane will add constructively and not cancel. This difference can be accounted for simply in terms of a factor of sin θ, and we show the orientation dependence of the envelope function for dipolar and quadrupolar terms in Figures 8 and distribution width dependence in Figures 9. For the calculations presented in Figures 9, we have convoluted the zero-degree tilt angle envelope functions shown in Figures 8 with a Gaussian width distribution of 1° and 10 to 70° in 10° increments.

We consider the nonlinear chromophore orientation dependence first. For a molecule with its nonlinear transition moment oriented along the surface normal, the minimum signal will occur for the electric field propagating along the surface normal axis. The orientation dependence of our data is manifested most prominently in the envelope function of the experimental data, as schematized in Figure 8a for the quadrupolar $\chi^{(2)}$ term and in Figure 8b for the dipolar $\chi^{(2)}$ term. It is clear from these calculations, based on eqs 1−4 and neglecting the optical interference effects, that the nonlinear chromophore orientation will have a more significant effect on the quadrupolar term than on the dipolar term due to the in-plane cancellation effect operative in the latter case.

To understand the limits inherent to the interpretation of our data, we need also to consider the effect of the chromophore orientational distribution width on the envelope function. The orientation distribution width dependence of the signal is described by the quantity D,[61]

$$D = \frac{\langle \cos^3 \theta \rangle}{\langle \cos \theta \rangle} \tag{7}$$

We show the effect of increasing orientational distribution width on the calculated envelope function for the quadrupolar term in Figure 9a and for the dipolar term in Figure 9b. These calculations are for a chromophore orientational distribution centered around the substrate normal. The broadening of the function near 0° tilt angle is reflective of the change in orientational distribution while the invariance of the signal near 70° demonstrates that, at high angles, the SSHG signal is dominated by optical considerations as described in eqs 4. On the basis of these calculations, it is clear that the unambiguous resolution of chromophore tilt angle and distribution width is limited by the S/N ratio of our data and the ability to separate the quadrupolar and dipolar terms experimentally.

We consider next the nonlinear optical properties of multilayers of each of the chromophores shown in Figure 1. Katz has reported previously on the second-order nonlinear response of chromophore **1**.[21] Our data are consistent with his and we observe a square-law dependence of the second harmonic intensity with increasing number of layers for both chromophores. This is an expected result for a system where the nonlinear medium is significantly thinner than the coherence length of the incident light source. The data we present in Figure 10a demonstrate this relationship and show that the system is sufficiently ordered to allow the square-law relationship to be manifest for both chromophores. We estimate $\chi^{(2)} = 4.0 \times 10^{-16}$ esu/cm^2-layer for **1** based on the experimental signal relative to that of the quartz substrate. Katz reported a value of $\beta = 150 \times 10^{-30}$ esu for a four-layer stack of **1** characterized by an order parameter of 0.2.[21] Assuming a layer density of 1.6 ×

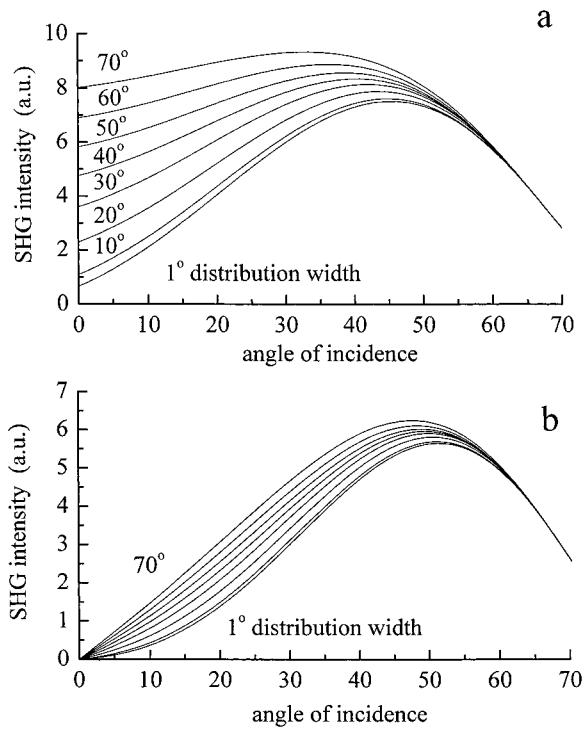

Figure 9. (a) Dependence of the envelope function on orientational distribution width for quadrupolar $\chi^{(2)}$ response. The distribution function is assumed to be Gaussian, and the chromophore average orientation is along the surface normal axis. (b) Dependence of the envelope function on orientational distribution width for dipolar $\chi^{(2)}$ response. The distribution function is assumed to be Gaussian, and the chromophore average orientation is along the surface normal axis.

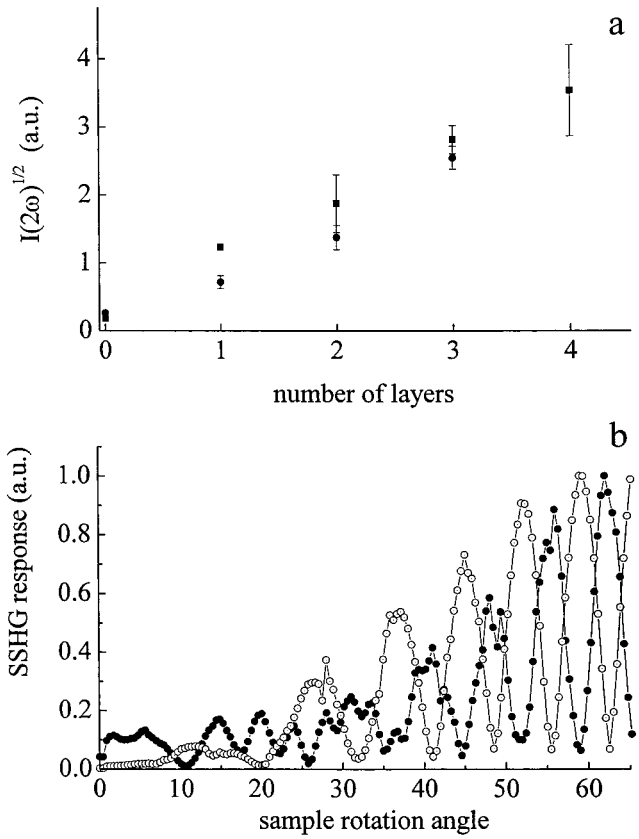

Figure 10. (a) Plot of the [SHG Intensity]$^{1/2}$ vs the number of chromophore layers. (b) Angle-dependent SSHG signals from chromophores **1** (●) and **2** (○). These data are dominated by substrate response at small angles and chromophore response at high angles.

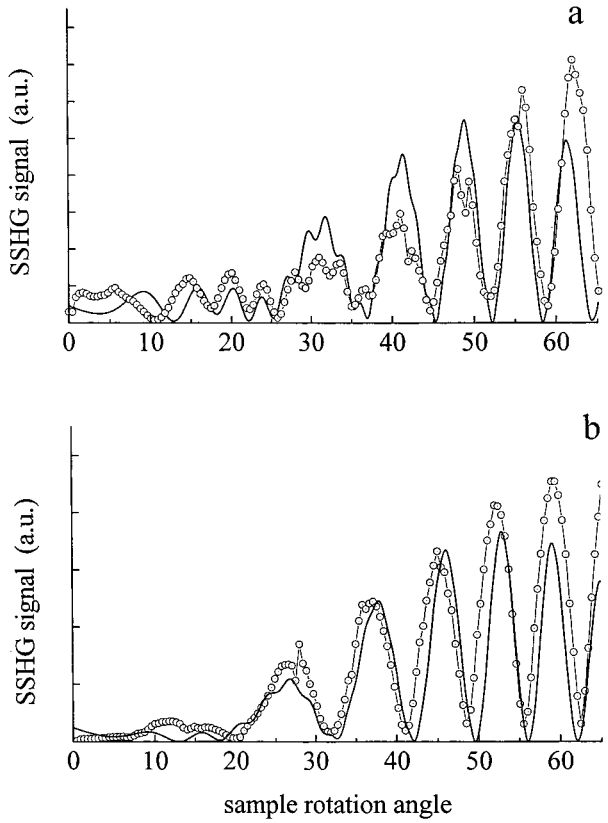

Figure 11. (a) Comparison of experimental SSHG data to the model presented in eqs 1−5 for chromophore **1**. (b) Comparison of data and calculations for chromophore **2**.

10^{14} cm^{-2} and the same layer order, our data correspond to a value of 200×10^{-30} esu.

There are many possible molecular and bulk contributions to the nonlinear response of the interfaces we study here, and based on the subtle differences in the linear response of **1** and **2**, it is possible that the magnitude of their $\chi^{(2)}$ responses could be different. From the data shown in Figure 10a, it is clear that the magnitudes of the $\chi^{(2)}$ responses for chromophores **1** and **2** are the same to within the experimental uncertainty. While the magnitudes are equal, the sign of the nonlinear response for these two chromophores is opposite owing to their complementary orientations, and this condition is apparent in the phase relationship of the angle-dependent SSHG data (Figure 10b).[52]

The experimental angle-dependent SSHG data for each chromophore can be modeled using eqs 1−5. We present the correspondence between the calculated response and the experimental response for a single layer of chromophore **1** in Figure 11a and for a single layer of chromophore **2** in Figure 11b. For both chromophores, the agreement between experiment and model is reasonable. For small sample rotation angles, the signal has a measurable contribution from the SiO_x substrate while at higher rotation angles the chromophore response dominates. For the chromophores, it is likely that the electric dipole contribution to their $\chi^{(2)}$ response is dominant, owing to their structures. As discussed above, the manner in which we acquire SSHG data is not amenable to precise orientation angle or distribution determinations, but it is clear from the experimental signals that the largest $\chi^{(2)}$ susceptibility terms for chromophore layers lie close to the substrate normal.

We now turn to the issue of assessing the nonlinear response of multilayer assemblies that contain both chromophores. For a bilayer system, there are two possible structural permutations: [SiO_x-**1**-**2**] and [SiO_x-**2**-**1**]. Before comparing their nonlinear responses, it is important to ensure that the formation of these bilayers does not give rise to anomalous changes in their linear response. The absorption spectra of both bilayers are identical to the linear responses of the individual chromophores. We present the $\chi^{(2)}$ data for these two bilayer structures in Figures 12a and 12b. The data include $\chi^{(2)}$ responses of the bare substrate before deposition for comparison. The most striking feature of these data is that the responses of the two complete bilayers are not the same. This result is reproducible and cannot be accounted for in the context of simple additivity of the constituent electric dipole contributions. If electric dipole or any other contribution(s) intrinsic to the chromophores and the substrate accounted for the overall $\chi^{(2)}$ response, the two bilayer structures would necessarily produce identical nonlinear responses, with any difference between the bilayer and bare substrate responses being attributable to vacancy and/or orientational defects. There may be some hint of this effect in the data in Figure 12a for high rotation angles, but this issue remains under investigation. We note that the cancellation we observe in these data demonstrates the feasibility of our approach to $\chi^{(2)}$ background nulling. Because the interlayer linking chemistry is the same for both bilayer structural permutations and the formation constant for ZP materials is characteristically so large, there is no reason to expect a difference for the bilayer responses based on differences in the efficiency of layer formation.

The fact that the bilayer data in Figures 12 are not identical demonstrates the importance of subtle structural contributions to the overall nonlinear response of the system. The only structural difference between the two bilayers lies in the region near where the two layers are connected through ZP linkages. It is known that the zirconium bisphosphonate solid-state

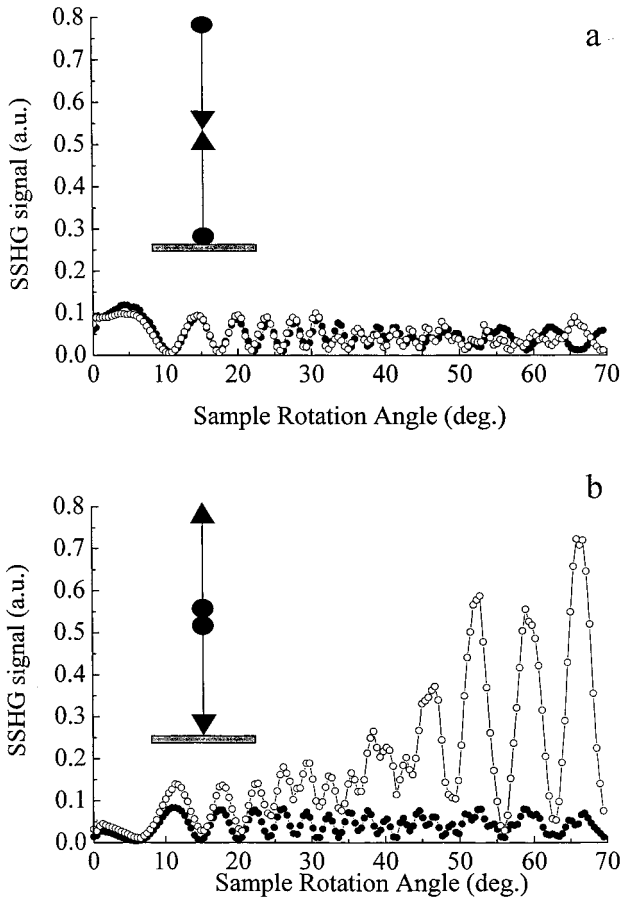

Figure 12. Surface SHG of (a) [SiO_x-**1**-**2**] and (b) [SiO_x-**2**-**1**] bilayers showing the cancellation of SHG signal with the adsorption of the second layer. The open circles are data on the bilayer structures, and the solid circles are SSHG data for the bare SiO_x substrates.

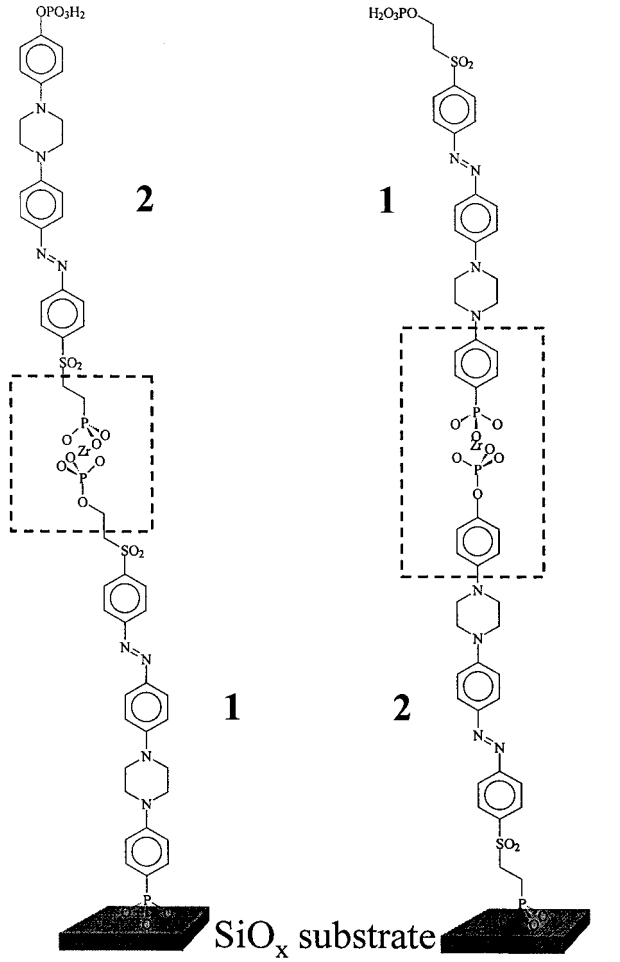

Figure 13. (a) Structure of [SiO_x-**1**-**2**] bilayer. (b) Structure of [SiO_x-**2**-**1**] bilayer. Note the structural difference between the interlayer linkages for the two assemblies (boxed).

structure possesses a center of inversion about the metal ion, ruling out an electric dipole allowed contribution to the signal from this moiety. At first glance, one could invoke the phosphate/phosphonate asymmetry to account for a $\chi^{(2)}$ response, but a more detailed examination of the bilayer structure reveals that this asymmetry is oriented in the same direction for both bilayer structures. The only structural difference between the two bilayers is the polarizability, and thus the hyperpolarizability, of the organic functionalities attached to the phosphate and phosphonate moieties. For [SiO_x-**1**-**2**], the interlayer **1**-**2** connection is of the form indicated in Figure 13a and for [SiO_x-**2**-**1**] the analogous structure is shown in Figure 13b. As indicated above, the net dipolar contributions should be the same for both structures, but the quadrupole moment for [SiO_x-**1**-**2**] should be substantially less than that for [SiO_x-**2**-**1**]. The electric quadrupole moment for [SiO_x-**2**-**1**] should be oriented along the chromophore tilt axis and both of these structurally based predictions are consistent with the experimental data. Unfortunately, there is no reliable means to estimate the magnitude of the nonlinear responses associated with these interlayer connecting structures. The central point is, however, that the nonlinear response of these bilayers cannot be accounted for simply by adding the dipolar contributions of the component parts.

Conclusion

We have synthesized and characterized Zr-phosphate/phosphonate (ZP) self-assembled multilayer structures using surface second harmonic generation measurements. We have used two $\chi^{(2)}$-active chromophores with complementary structures and have assembled bilayers with controlled orientation relative to the substrate. The nonlinear optical responses of the SiO_x substrate and of multilayers of each of the chromophores have been characterized. For the substrate we find substantial contributions to the nonlinear response from the electric quadrupole contributions to the total $\chi^{(2)}$ term, in agreement with the work of Guyot-Sionnest and Shen.[60] For each chromophore, multilayer structures provide the expected dependence of second harmonic signal on number of layers and, based on the magnitudes of these signals, the electric dipole term likely dominates the chromophore $\chi^{(2)}$ responses. Using these same chromophores, we have formed bilayers to produce two different, canceling structural motifs, each with a local center of inversion about the ZP interlayer bonding plane. The $\chi^{(2)}$ responses of the two bilayer systems are measurably different, revealing the limitations of accounting for nonlinear optical responses simply in terms of additive contributions from the constituents. The differences in the nonlinear responses of the two systems can be accounted for through cancellation of the electric dipole contribution to $\chi^{(2)}$, with the residual difference arising from the electric quadrupole contribution. This higher order response is associated with the region centered around the interlayer linking group. Our data underscore the complex and nonadditive issues associated with the design and construction of layered interfaces and, in principle, provide a means to measure the vacancy defect density in layered materials. Clearly the chromophores we have used in this report are not ideal

candidates for vacancy defect density measurements, but simple synthetic means can be used to improve their utility for this application. These data also raise the issue of the thickness of interface that SSHG measurements are sensitive to, and we anticipate future work in this area to shed new light on this matter.

Acknowledgment. We gratefully acknowledge the National Science Foundation and the donors of the Petroleum Research Fund, administered by the American Chemical Society, for support of this work. We wish to thank AT&T Bell Laboratories for their generous donation of the laser system.

Supporting Information Available: Synthetic route to chromophore **2**. This material is available free of charge via the Internet at http://pubs.acs.org.

JA000232Y